Ligand-mediated microenvironment tuning of UiO-66 to boost Pt activity for efficient VOCs oxidation

Juntian Li [a], Changjian Wang [a], Didi Li [b], Zhimin Ao [a*]

[a] *Guangdong Provincial Key Laboratory of Wastewater Information Analysis and Early Warning, Advanced Interdisciplinary Institute of Environment and Ecology, School of Technology for Sustainability, Beijing Normal University, Zhuhai 519087, China;*

[b] *School of Environmental Science and Engineering, Guangdong University of Technology, Guangzhou 510006, China.*

[*] Correspondence to: Zhimin Ao. E-mail address: zhimin.ao@bnu.edu.cn.

Keywords: Metal-organic frameworks; Microenvironment modulation; Metal-support interaction; Volatile organic compounds; Backpropagation neural network.

Materials and Methods

Figure S1 The pore width distribution of UiO-66-0, UiO-66-5, UiO-66-10 and UiO-66-15.

Figure S2 The toluene in-situ DRIFTs of UiO-66-0 at 25 ºC over time.

Figure S3 The toluene in-situ DRIFTs of UiO-66-5 at 25 ºC over time.

Figure S4 The toluene in-situ DRIFTs of UiO-66-10 at 25 ºC over time.

Figure S5 The toluene in-situ DRIFTs of UiO-66-15 at 25 ºC over time.

Figure S6 The toluene in-situ DRIFTs of UiO-66-0, UiO-66-5, UiO-66-10 and UiO-66-15 at 50 ºC.

Figure S7 TEM characterizations of the synthesized UiO-66-0.

Figure S8 TEM characterizations of the synthesized UiO-66-5.

Figure S9 TEM characterizations of the synthesized UiO-66-10.

Figure S10 TEM characterizations of the synthesized UiO-66-15.

Figure S11 BET curves of Pt/UiO-66-0, Pt/UiO-66-5, Pt/UiO-66-10 and Pt/UiO-66-15.

Figure S12 The pore width distribution of Pt/UiO-66-0, Pt/UiO-66-5, Pt/UiO-66-10 and Pt/UiO-66-15.

Figure S13 Catalytic performance of UiO-66-10 for toluene oxidation.

Figure S14 Catalytic performance of different Pt-supported catalysts for toluene oxidation.

Figure S15 Catalytic performance of Pt/UiO-66-10 for the catalytic degradation of toluene for 48 hours at 170 °C.

Figure S16 Catalytic performance of Pt/UiO-66-10 for the catalytic degradation of toluene in three cycles.

Figure S17 BPNN-predicted relative contributions of UiO-66 intrinsic properties to the O_{ads}/O_{latt} ratio and Zr 3d shift in Pt/UiO-66.

Figure S18 BPNN-predicted relative contributions of Pt/UiO-66 intrinsic properties to toluene conversion.

Figure S19 Comparison between the experimental data and the predicted results.

Table S1 BET surface area, pore volume, pore width and toluene adsorption capacity

of UiO-66-0, UiO-66-5, UiO-66-10 and UiO-66-15.

Table S2 BET surface area, pore volume, pore width and Pt loading of Pt/UiO-66-0, Pt/UiO-66-5, Pt/UiO-66-10 and Pt/UiO-66-15.

Table S3 Intermediate products measured by PTR-TOF-MS for toluene oxidation of Pt/UiO-66-10.

Materials and Methods

Chemicals

Zirconium chloride ($ZrCl_4$, 98%) was purchased from Acros Organics. Chloroplatinic acid hexahydrate ($H_2PtCl_6 \cdot 6H_2O$, ACS reagent, 37.5% Pt basis) were purchased from Sigma-Aldrich. Acetic Acid (99.8%), benzoic acid (99.5%)，4,4'-Bibenzoic Acid (97%) and 1,3,5-benzenetricarboxylic acid (BTC, 97%) was purchased from Aladdin. Terephthalic acid (H_2BDC, 99%) and Ethanol (99.7%) were purchased from Macklin. N, N-dimethylformamide (DMF, 99.8%) and methanol (99.9%) were purchased from Fisher chemical.

Methods

Synthesis of UiO-67

$ZrCl_4$ (0.636 g, 2.729 mmol), 4,4′-biphenyldicarboxylic acid (0.66 g, 2.729 mmol) and benzoic acid (3.936 g, 27.29 mmol) were dissolved in 60 mL of DMF. The mixture was sonicated for 10 min, then transferred to a reaction vessel and heated in a pre-heated oven at 120 °C for 24 h. After cooling to room temperature, the product was collected by centrifugation, washed three times each with DMF and ethanol, and subsequently subjected to solvent exchange with methanol. During the exchange, the methanol was replaced with fresh solvent every 8 h, and the process was repeated three times.

Synthesis of MOF-808

$ZrCl_4$ (1.05 g, 4.5 mmol) was dissolved in 45 mL of acetic acid (99.5%) and sonicated for 30 min. Separately, 1,3,5-benzenetricarboxylic acid (BTC, 0.31 g, 1.5 mmol) was dissolved in 45 mL of DMF and sonicated for 30 min. The two solutions

were combined after sonication, transferred into a polytetrafluoroethylene (PTFE)-lined reaction vessel, and heated at 120 °C for 72 h. After cooling to room temperature, the resulting mixture was centrifuged to isolate MOF-808. The product was subsequently washed four times with acetone under ultrasonication, followed by centrifugation at 11000 rpm each time. Finally, the solid was dried at 100 °C for over 12 h.

Synthesis of Pt/UiO-67 and Pt/MOF-808.

Pt/Zr-MOFs (Zr-MOFs = UiO-67 and MOF-808) were prepared using an incipient wetness impregnation approach. First, the as-synthesized Zr-MOFs were activated under vacuum at 120 °C for 8 h. Subsequently, 200 mg of the activated support was dispersed in methanol in a 50 mL screw-cap vial by ultrasonication. To this dispersion, 1 mL of $H_2PtCl_6 \cdot 6H_2O$ solution was added, and the mixture was stirred for 1 h. Thereafter, 40 mg of $NaBH_4$ solution was introduced, followed by continuous stirring for 30 min. The resulting solid was collected by high-speed centrifugation (11000 rpm, 5 min) and washed three times under the same conditions. Finally, the product was vacuum-dried at 40 °C for 12 h and stored in a desiccator under vacuum prior to further use.

Backpropagation neural network (BPNN)

Relative contributions of UiO-66 intrinsic properties to the O_{ads}/O_{latt} ratio and Zr 3d shift in Pt/UiO-66: To establish quantitative structure-activity relationships for the catalysts, backpropagation artificial neural network (BPNN) models were developed using Python with scikit-learn libraries. A single-hidden-layer backpropagation neural network architecture was implemented, utilizing grid search with cross-validation for hyperparameter optimization. The models incorporated sigmoid activation functions for non-linear mapping and employed the Adam optimization algorithm with early stopping to prevent overfitting. Feature importance analysis was performed using connection weight methodology to identify key structural determinants affecting catalytic performance. For the multi-output prediction with limited samples, leave-

one-out cross-validation was implemented to ensure model robustness, and separate importance analyses were conducted for each output variable.

Relative contributions of Pt/UiO-66 intrinsic properties to toluene conversion: To predict the catalytic performance of Pt/UiO-66 catalysts, a single-layer BPNN model was developed. Three structural parameters (O_{ads}/O_{latt} ratio, Pt^{2+}/Pt^{0} ratio, and Zr 3d shift) and reaction temperature were selected as input variables, with catalytic activity as the output target. The BPNN model comprises one hidden layer containing [optimal number] neurons, determined through comprehensive grid search optimization. Each neuron processes input signals through weighted connections, mathematically expressed as:

$$y_j = \sum_{i=1}^{n} \left(w_{ij} \times x_{ij} + b_j \right)$$

where w_{ij} represents the synaptic weight between the i-th input and j-th neuron, x_i denotes the input variable, and b_j is the bias term. To capture non-linear relationships, the hidden layer output is processed through a sigmoid activation function:

$$\sigma(x) = \frac{1}{1 + e^{-x}}$$

The output layer employs a linear activation function. The Adam optimization algorithm adaptively adjusts the learning rate during training, with weight updates incorporating momentum:

$$\Delta w_{ij}^{(s)} = -\eta \cdot \frac{\partial E}{\partial w_{ij}} + \mu \cdot \Delta w_{ij}^{(s-1)}$$

where $\Delta w_{ij}^{(s)}$ is the weight adjustment at the s-th iteration, η represents the learning rate (optimized around 0.01), E denotes the mean squared error loss function, and μ is the momentum factor. Grid search methodology was implemented to

optimize hyperparameters including hidden neuron count (2-5), learning rate (0.005-0.03), and maximum iterations (100-500), with early stopping to prevent overfitting. Set a random seed to ensure the repeatability of the results.

Multi-output regression with limited samples: A similar BPNN architecture was employed for the multi-output prediction of both O_{ads}/O_{latt} and Zr_3d_shift using four input parameters. Key distinctions include: (1) simultaneous prediction of dual output variables, (2) implementation of leave-one-out cross-validation (LOOCV) to address limited sample size (n=4), and (3) optimization of reduced hyperparameter ranges (hidden neurons: 1-3; learning rate 0.015-0.03) through grid search. The L-BFGS solver was utilized for enhanced stability with small datasets, and feature importance analysis was conducted separately for each output variable.

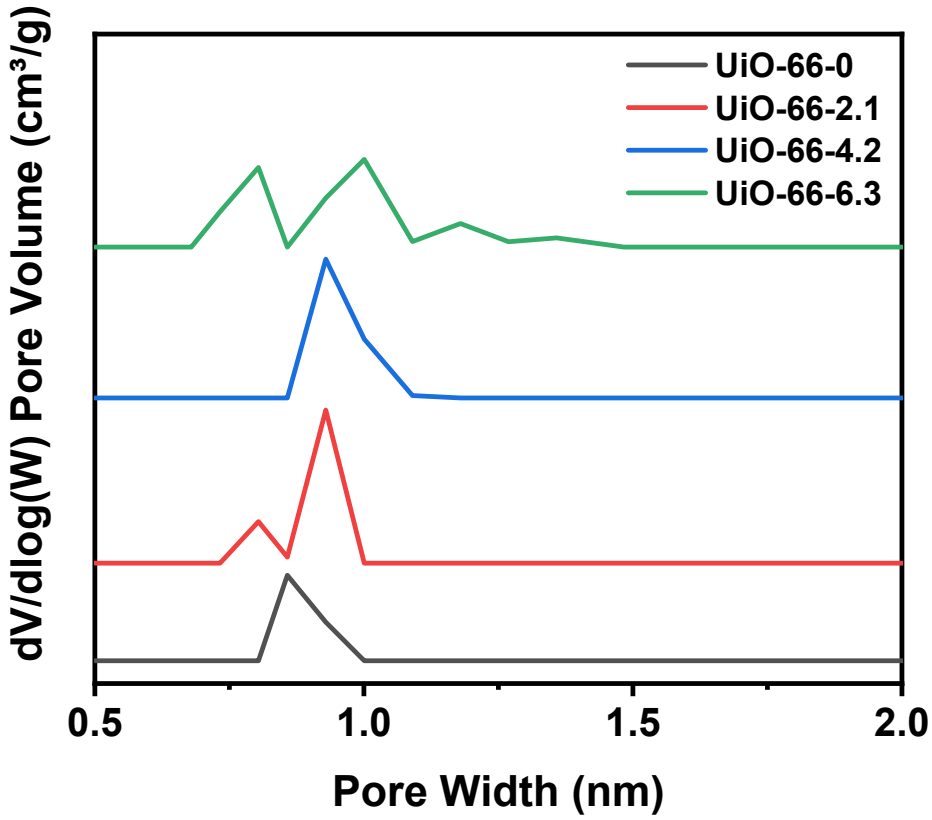

Figure S1. The pore width distribution of UiO-66-0, UiO-66-5, UiO-66-10 and UiO-66-15.

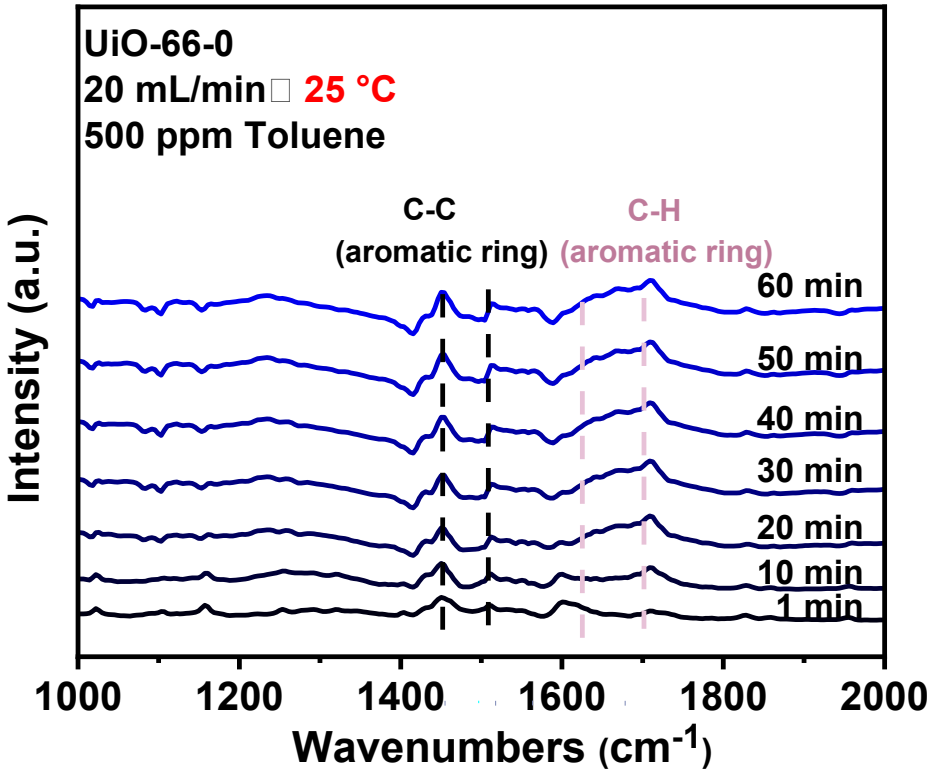

Figure S2. The toluene in-situ DRIFTs of UiO-66-0 at 25 ºC over time.

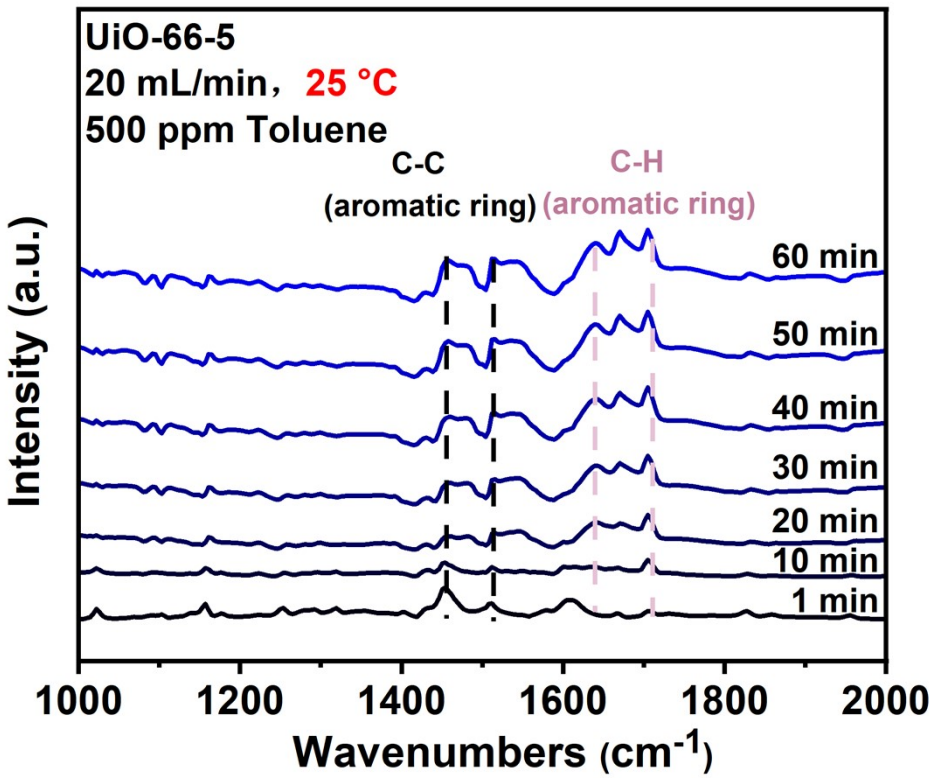

Figure S3. The toluene in-situ DRIFTs of UiO-66-5 at 25 ºC over time.

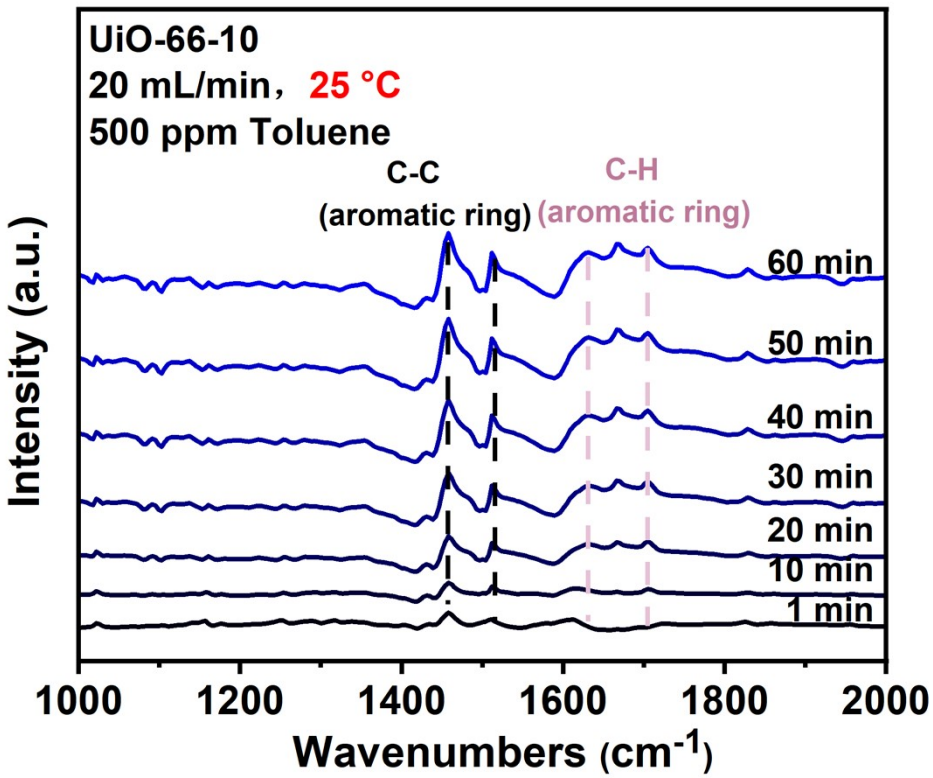

Figure S4. The toluene in-situ DRIFTs of UiO-66-10 at 25 ºC over time.

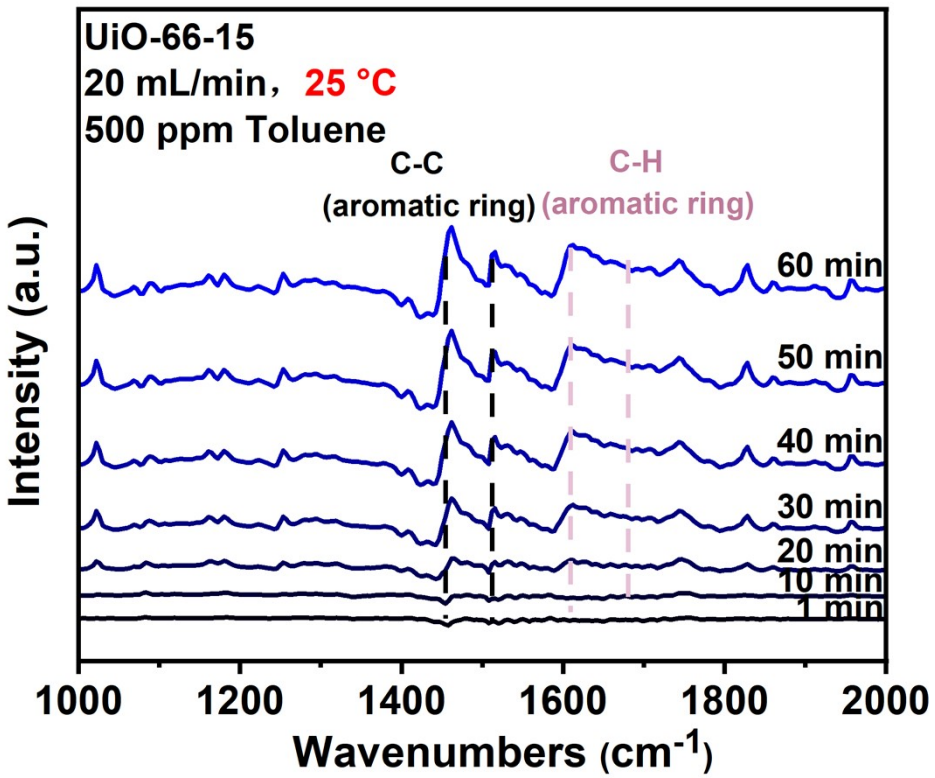

Figure S5. The toluene in-situ DRIFTs of UiO-66-15 at 25 ºC over time.

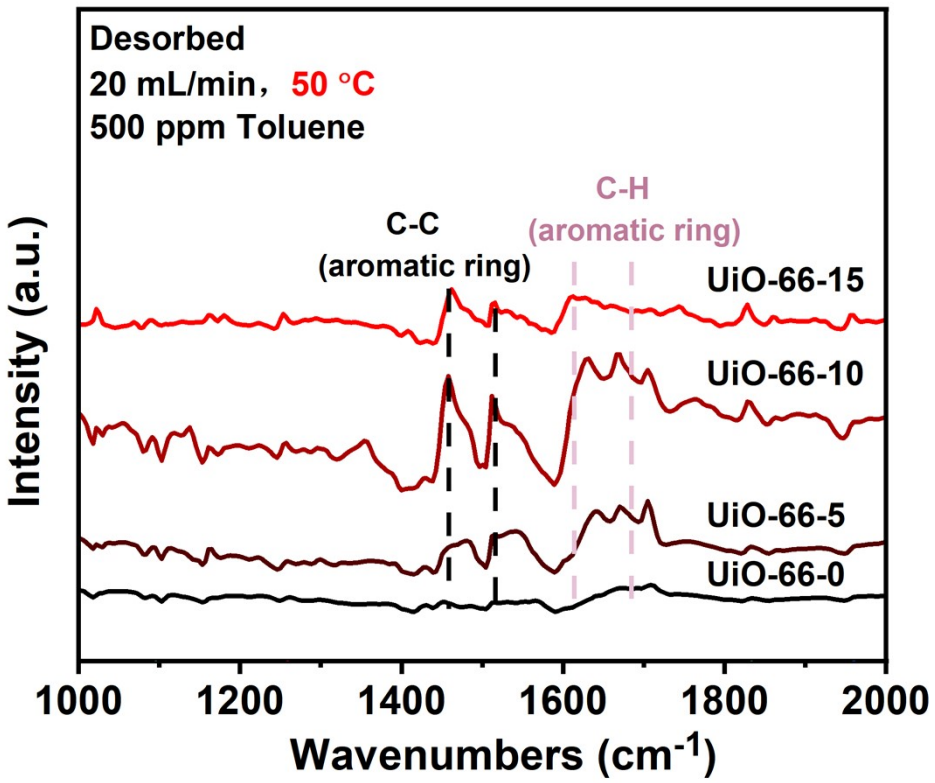

Figure S6. The toluene in-situ DRIFTs of UiO-66-0, UiO-66-5, UiO-66-10 and UiO-66-15 at 50 ºC.

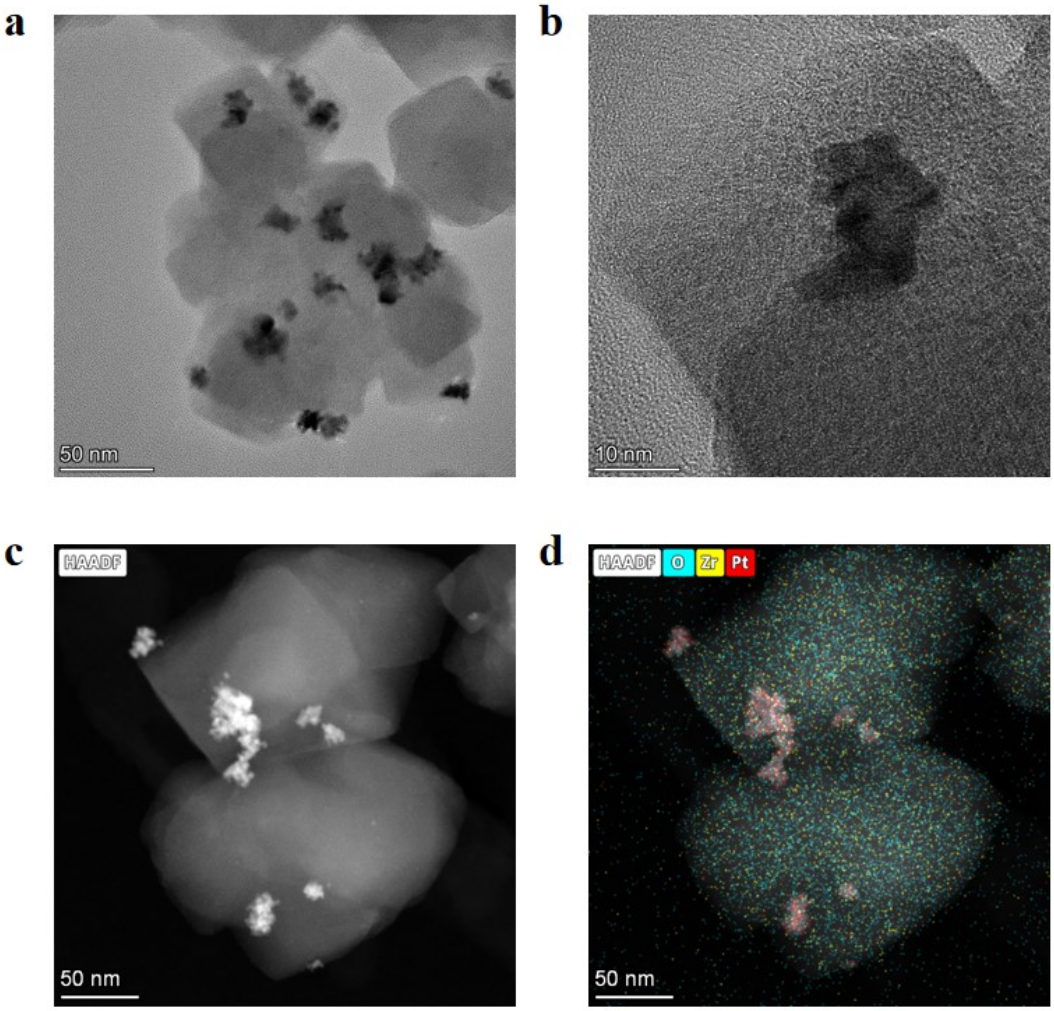

Figure S7. Characterizations of the synthesized Pt/UiO-66-0: (a) TEM image of the synthesized Pt/UiO-66-0 (scare bar: 50 nm). (b) TEM image of the synthesized Pt/UiO-66-0 (scare bar: 10 nm). (c) HAADF image of the synthesized Pt/UiO-66-0. (d) Mapping image of the synthesized Pt/UiO-66-0.

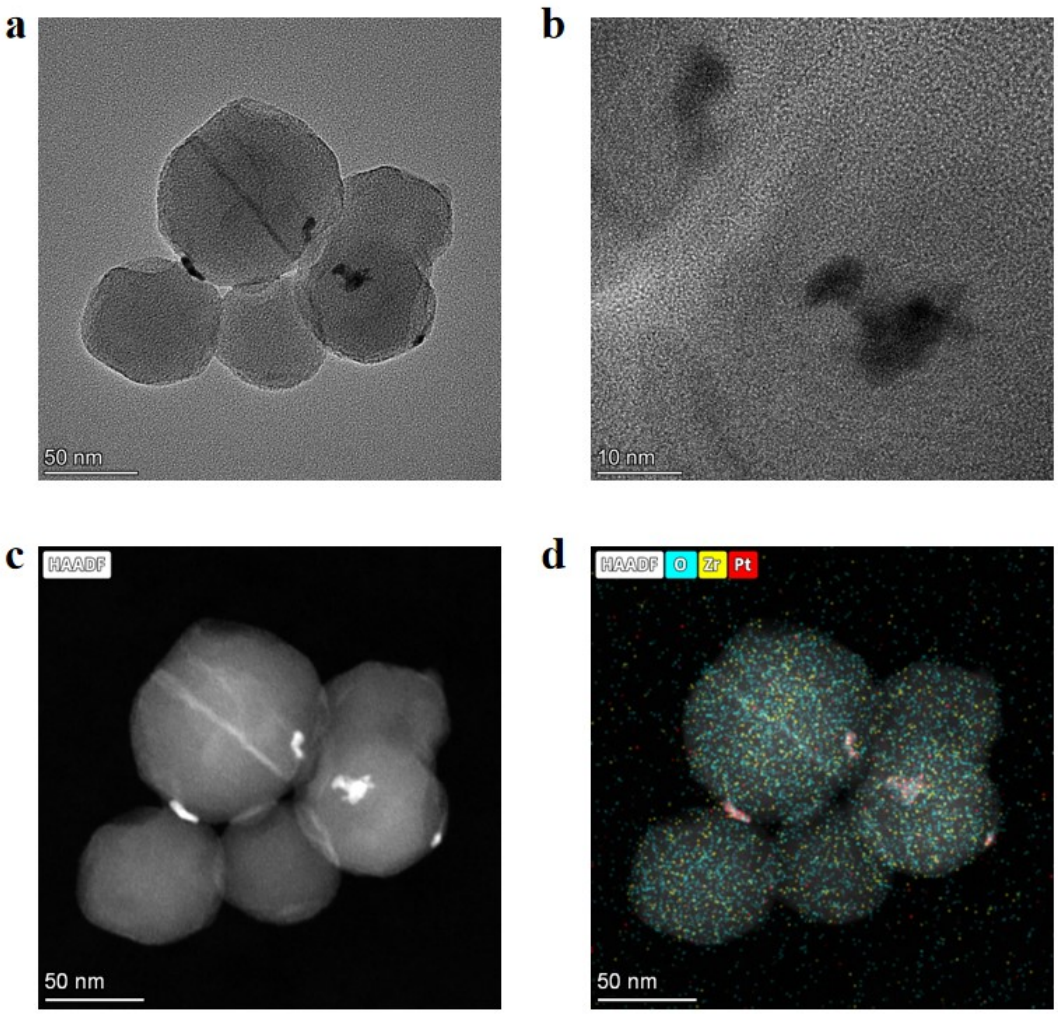

Figure S8. Characterizations of the synthesized Pt/UiO-66-5: (a) TEM image of the synthesized Pt/UiO-66-5 (scare bar: 50 nm). (b) TEM image of the synthesized Pt/UiO-66-5 (scare bar: 10 nm). (c) HAADF image of the synthesized Pt/UiO-66-5. (d) Mapping image of the synthesized Pt/UiO-66-5.

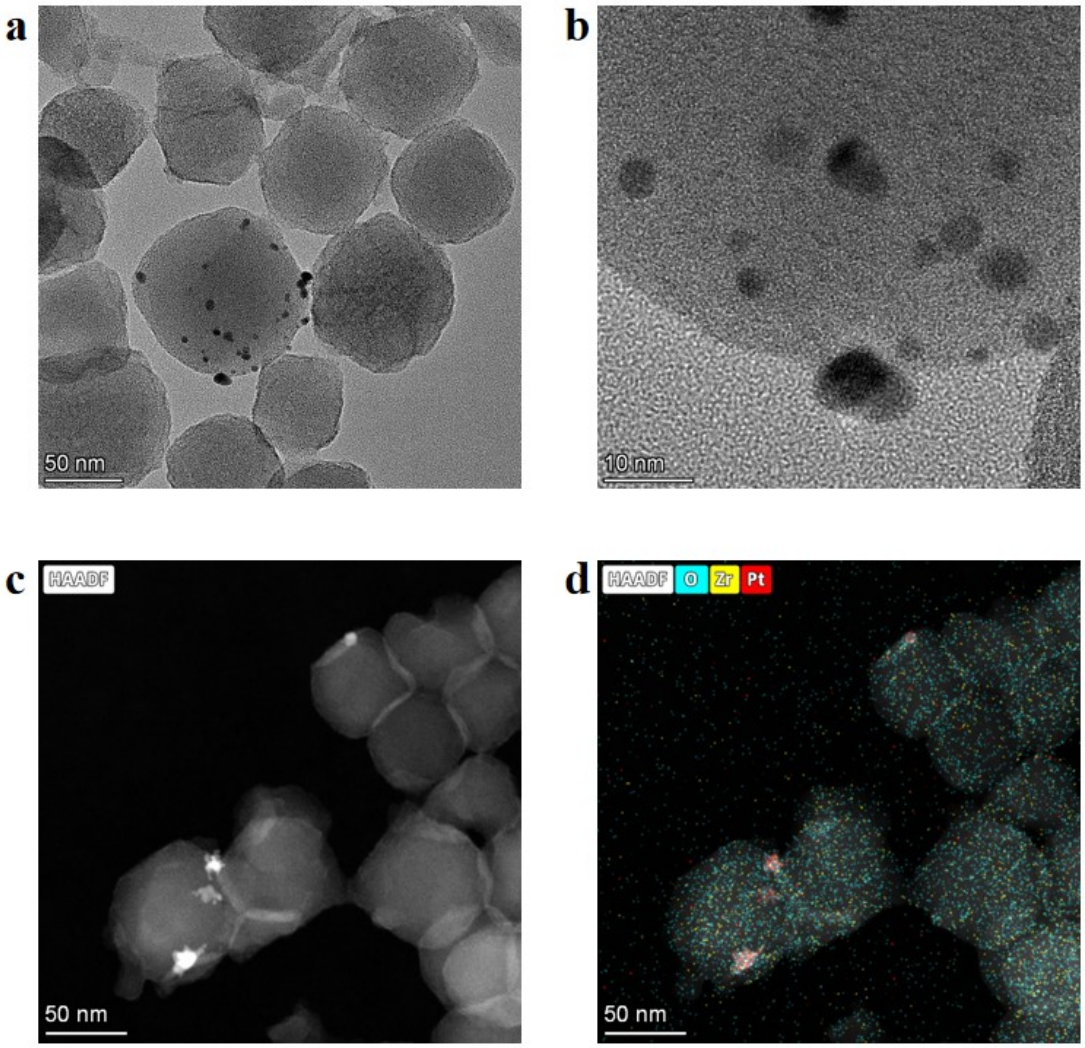

Figure S9. Characterizations of the synthesized Pt/UiO-66-10: (a) TEM image of the synthesized Pt/UiO-66-10 (scare bar: 50 nm). (b) TEM image of the synthesized Pt/UiO-66-10 (scare bar: 10 nm). (c) HAADF image of the synthesized Pt/UiO-66-10. (d) Mapping image of the synthesized Pt/UiO-66-10.

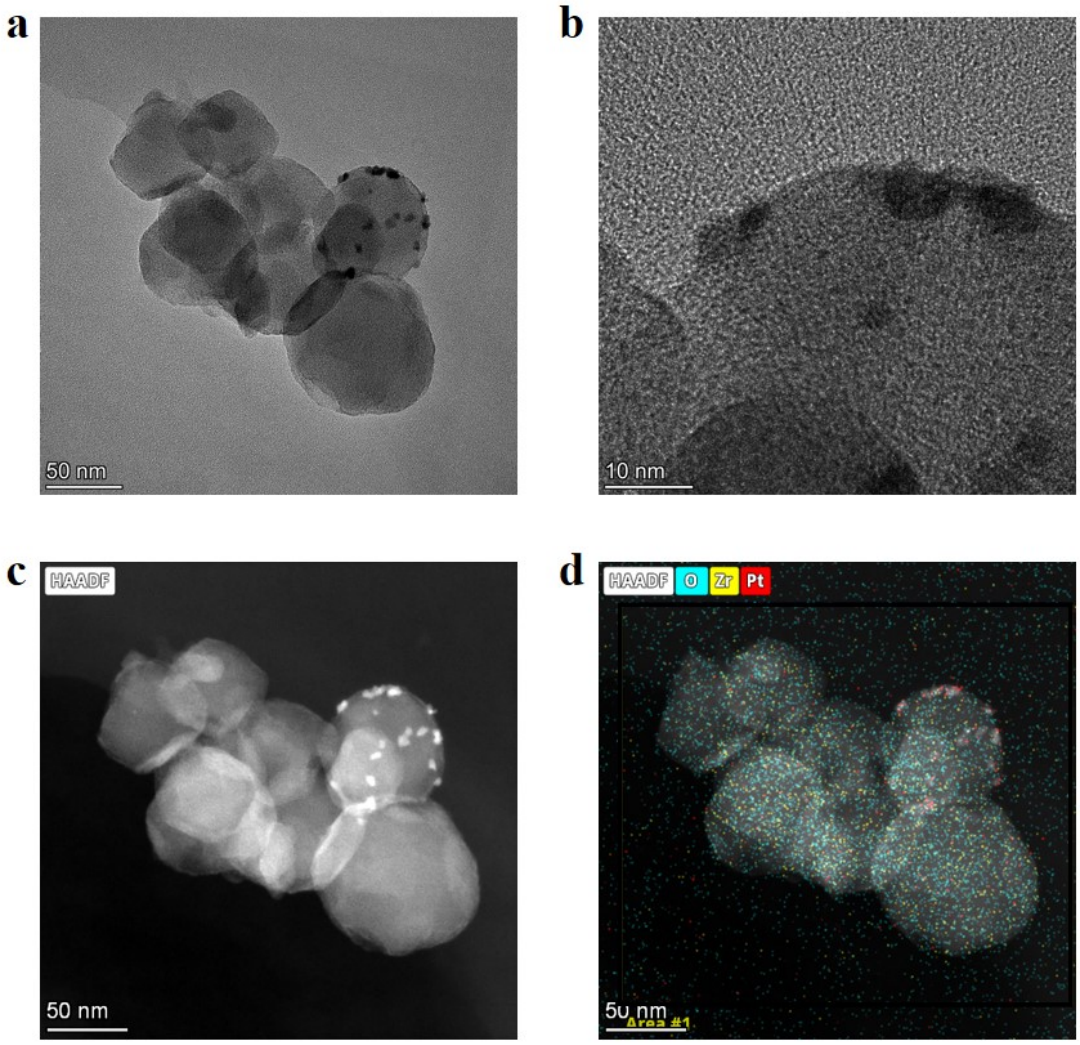

Figure S10. Characterizations of the synthesized Pt/UiO-66-15: (a) TEM image of the synthesized Pt/UiO-66-15 (scare bar: 50 nm). (b) TEM image of the synthesized Pt/UiO-66-15 (scare bar: 10 nm). (c) HAADF image of the synthesized Pt/UiO-66-15. (d) Mapping image of the synthesized Pt/UiO-66-15.

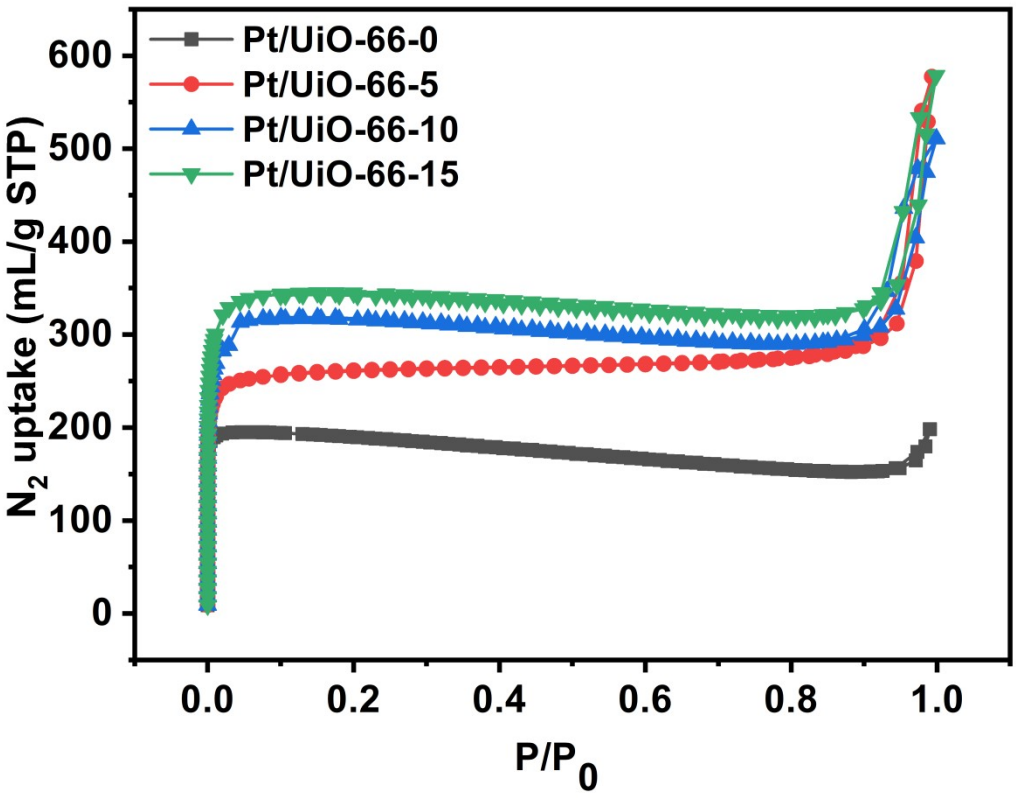

Figure S11. BET curves of Pt/UiO-66-0, Pt/UiO-66-5, Pt/UiO-66-10 and Pt/UiO-66-15.

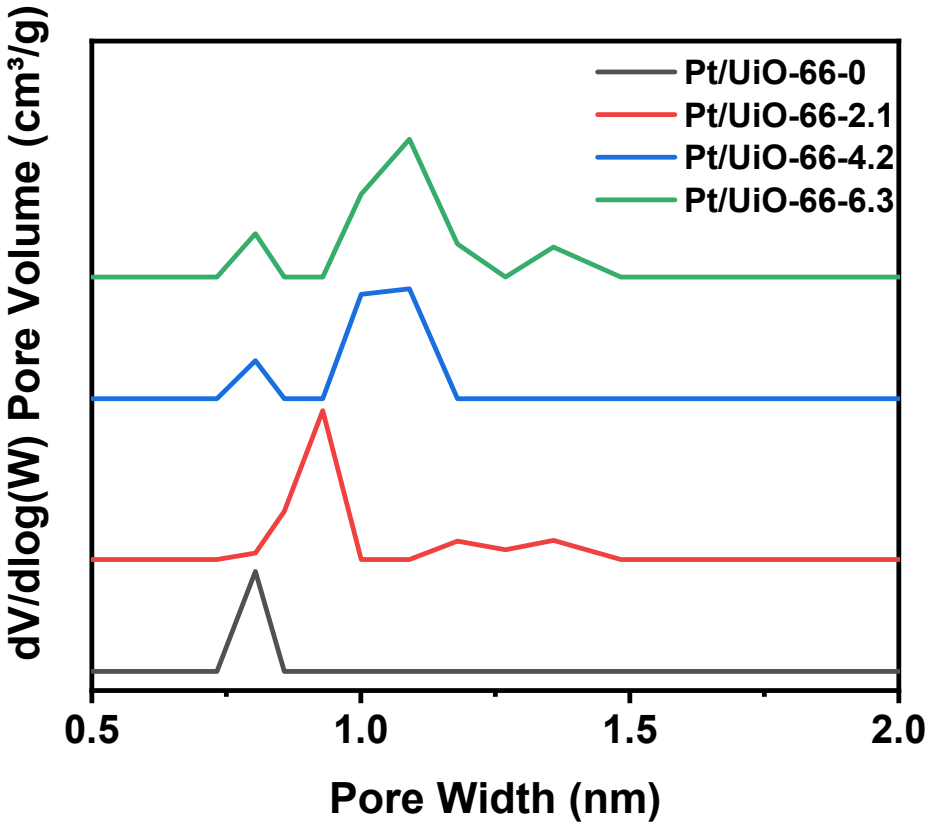

Figure S12. The pore width distribution of Pt/UiO-66-0, Pt/UiO-66-5, Pt/UiO-66-10 and Pt/UiO-66-15.

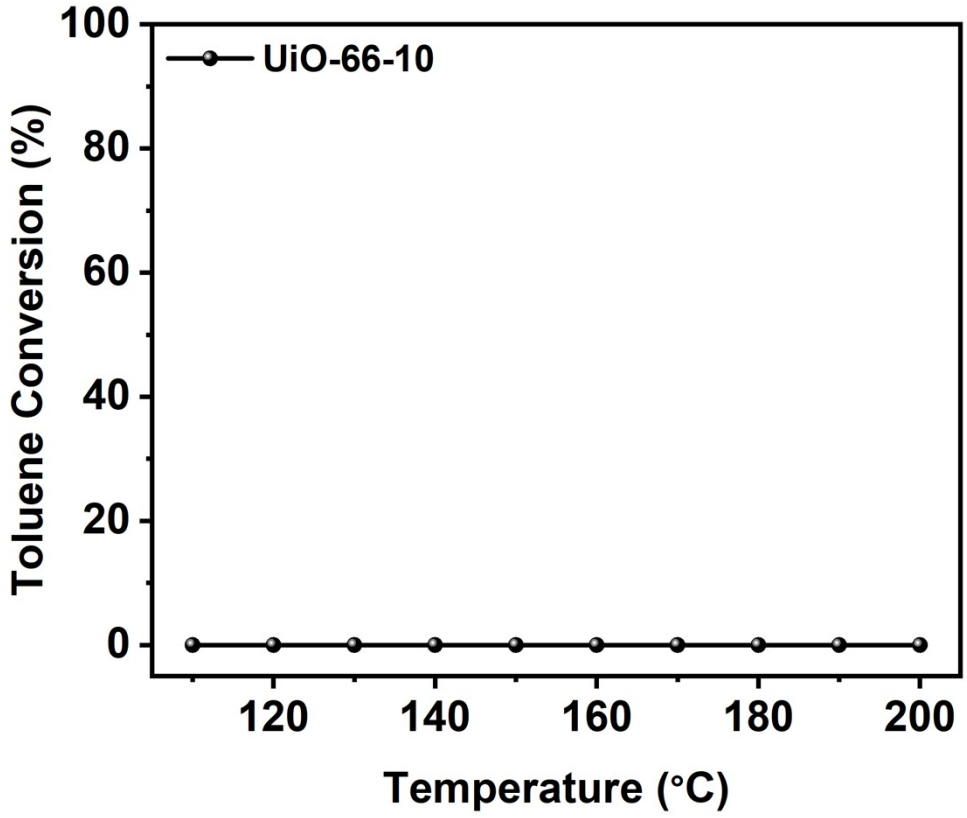

Figure S13. Catalytic performance of UiO-66-10 for toluene oxidation.

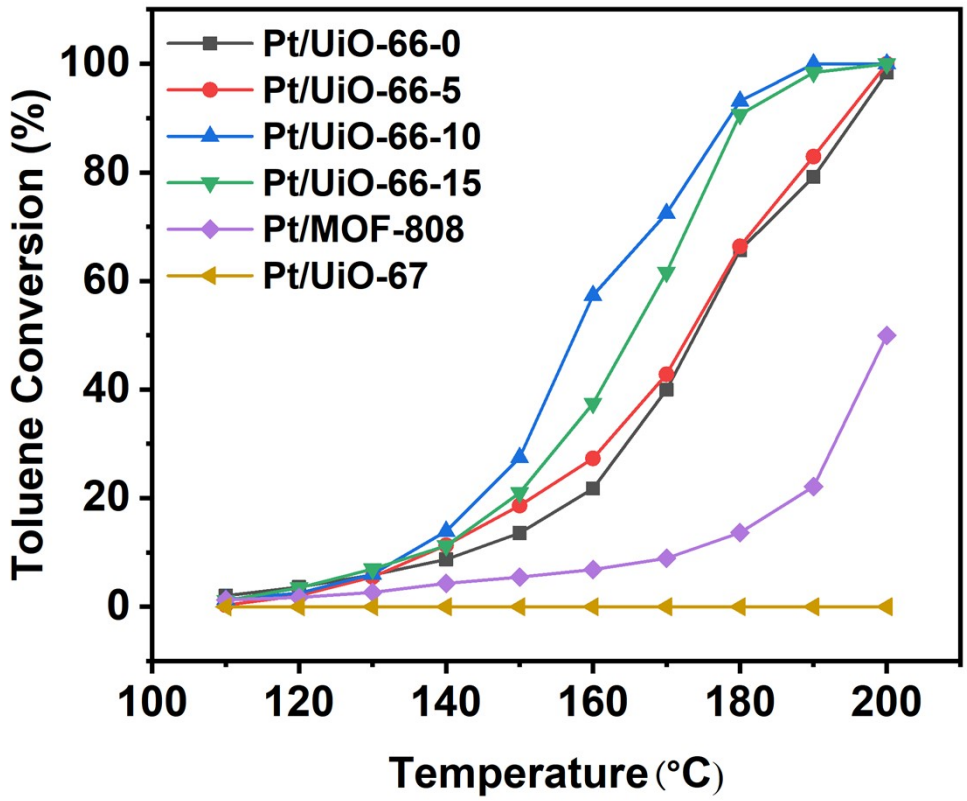

Figure S14. Catalytic performance of different Pt-supported catalysts for toluene oxidation.

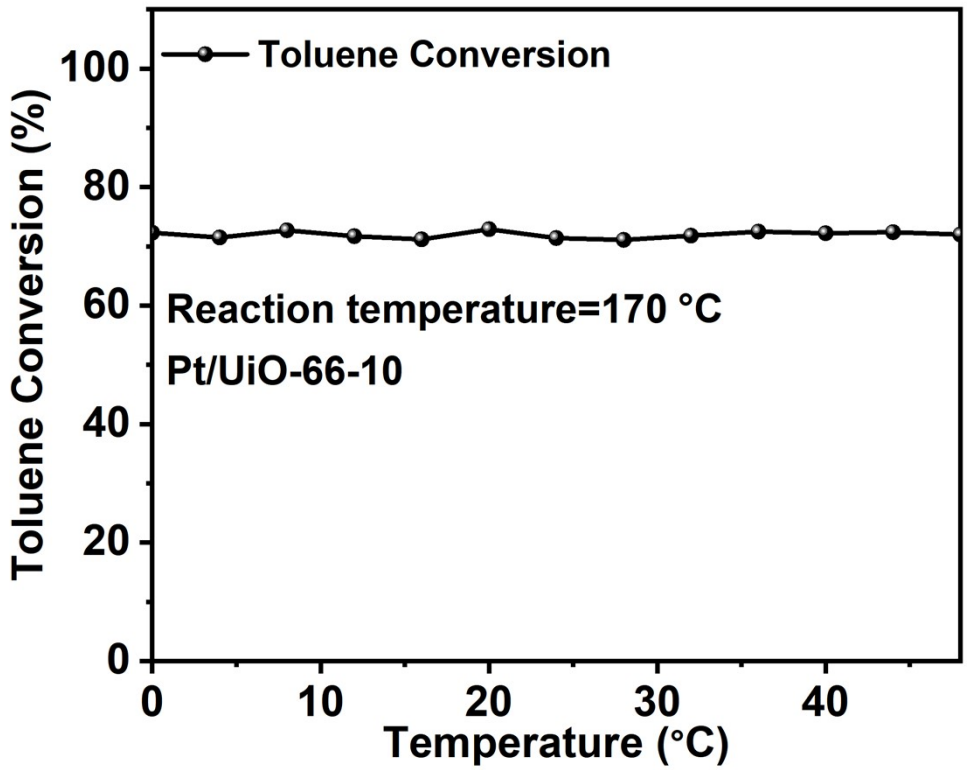

Figure S15. Catalytic performance of Pt/UiO-66-10 for the catalytic degradation of toluene for 48 hours at 170 °C.

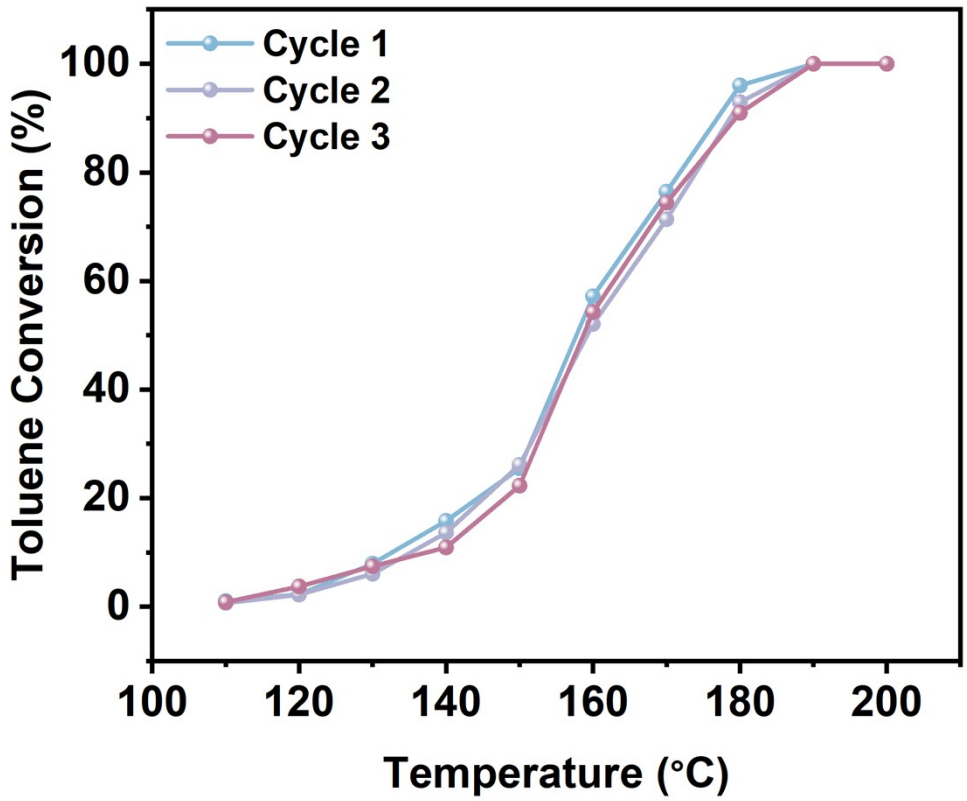

Figure S16. Catalytic performance of Pt/UiO-66-10 for the catalytic degradation of toluene in three cycles.

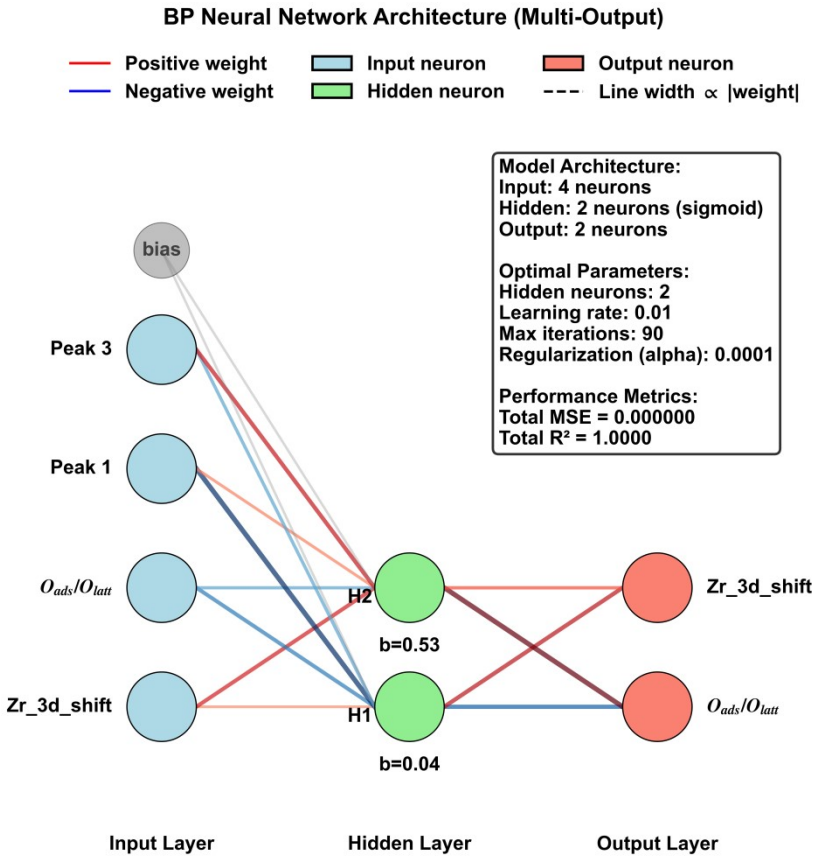

Figure S17. BPNN-predicted relative contributions of UiO-66 intrinsic properties to the O_{ads}/O_{latt} ratio and Zr 3d shift in Pt/UiO-66.

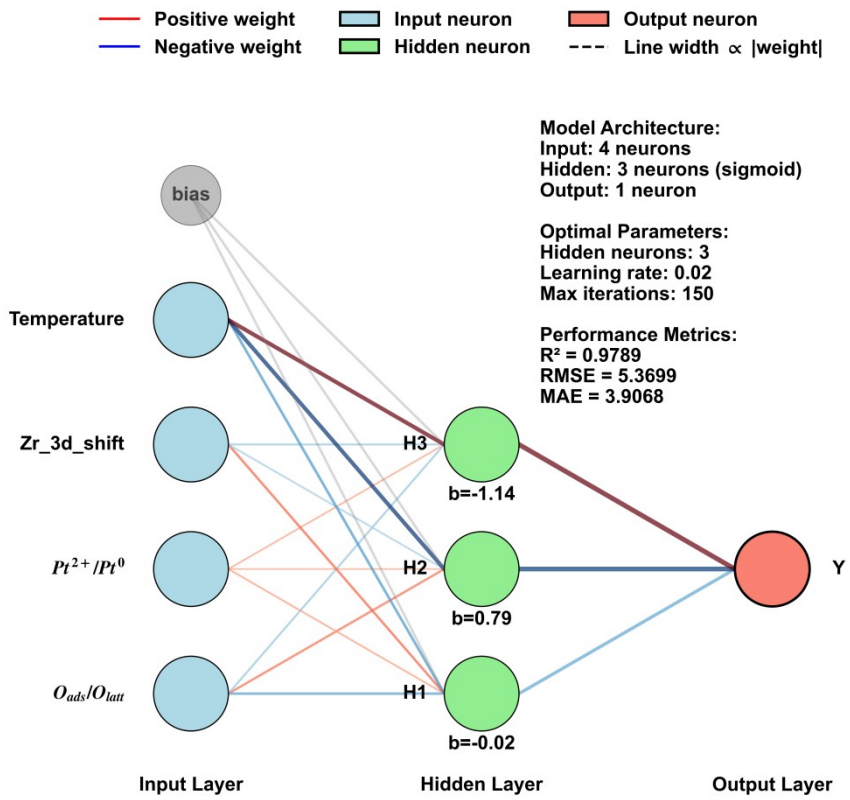

Figure S18. BPNN-predicted relative contributions of Pt/UiO-66 intrinsic properties to toluene conversion.

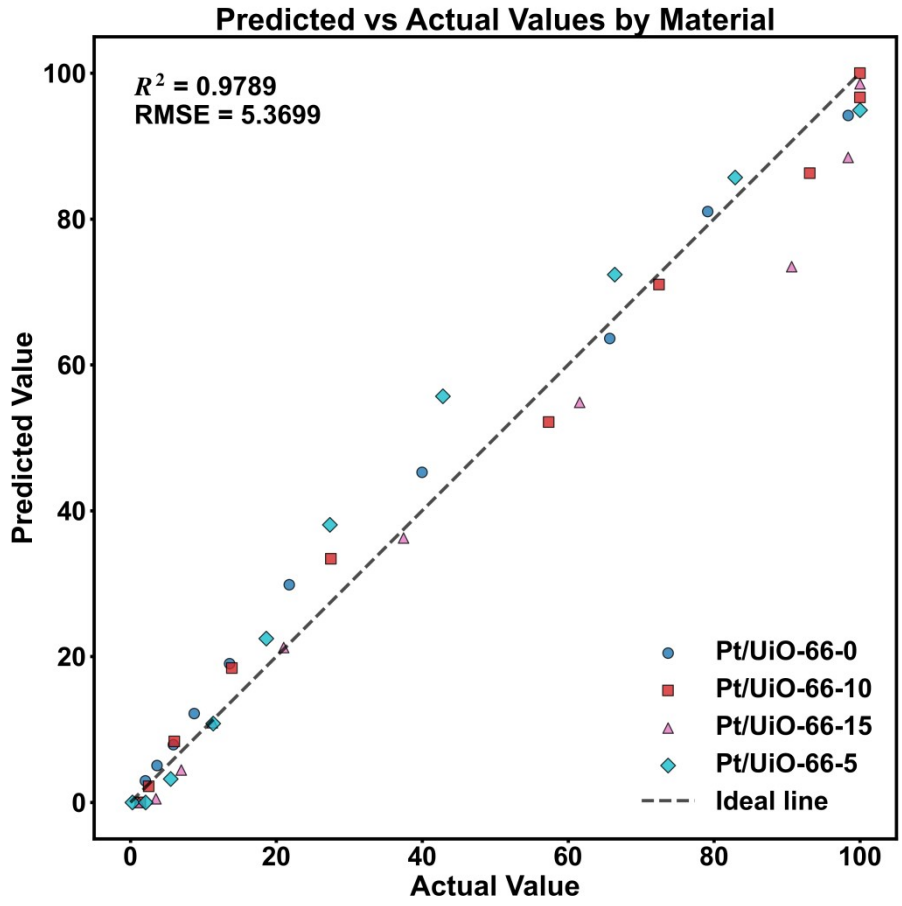

Figure S19. Comparison between the experimental data and the predicted results.

Table S1 BET surface area, pore volume, pore width and toluene adsorption capacity of UiO-66-0, UiO-66-5, UiO-66-10 and UiO-66-15.

catalysts	BET surface area （m^2/g)	Pore width （nm）	Toluene adsorption capacity (mg/g)
UiO-66-0	663.4458	0.8187	163
UiO-66-5	942.9711	0.8367	215
UiO-66-10	1017.1917	0.8643	238
UiO-66-15	1055.7066	0.8899	244

Table S2 BET surface area, pore volume, pore width and Pt loading of Pt/UiO-66-0, Pt/UiO-66-5, Pt/UiO-66-10 and Pt/UiO-66-15.

catalysts	BET surface area (m^2/g)	Pore width (nm)	Pt loading (.wt%)
Pt/UiO-66-0	563.1066	0.7992	1.10
Pt/UiO-66-5	786.7500	0.8374	1.03
Pt/UiO-66-10	999.6186	0.8796	0.91
Pt/UiO-66-15	1024.3412	0.9136	1.08

Table S3 Intermediate products measured by PTR-TOF-MS for toluene oxidation of Pt/UiO-66-10.

VOCs	m/z (VOCsH+)	Reaction temperature				
		120	140	160	180	200
Toluene	93.07	+	+	+	+	+
Benzylalcohol	109.07	+	+	-	-	-
Benzaldehyde	107.05	+	+	+	+	+
Benzoic acid	123.04	-	-	-	-	+
Phenol	95.05	+	+	+	+	+
Maleic Anhydride	99.10	+	+	+	+	+

+ represents existence, - represents difficult to detect or non-existent.